Sensor and Simulation Notes

Note 445

17 July 2000

**Compensation of an Electrically Large Coaxial
Transmission Line Bend by a Layered Dielectric Lens**

W. Scott Bigelow and Everett G. Farr
Farr Research, Inc.

William D. Prather
Air Force Research Laboratory, Directed Energy Directorate

Abstract

A 90° bend in an electrically large coaxial transmission line has been successfully compensated by a layered approximation of a cylindrically inhomogeneous dielectric (CID) lens. An equivalent straight length of line transmits an impulse with a width of 55 ps. Without compensation, the bend spreads the same signal over more than 500 ps. When compensated by the layered lens, the bend transmits the impulse with a width of only 70 ps.

This paper describes the design and testing of the layered dielectric lens. In an appendix, an objective function is defined for use in identifying globally optimal designs, subject to applicable constraints. The lens design documented here was found nearly optimal. Other bend compensation attempts, based on partially filling the transmission line cross section with a uniform dielectric material, are also documented. Those attempts were not successful.

1.   Introduction

This note presents our latest implementation of an electrically large transverse electro-magnetic (TEM) transmission line bend compensated by a layered approximation of a gradient index dielectric lens. As we have observed previously [1 and 2], a bend in an electrically large geometry poses a problem for ultra-wideband (UWB) impulse transmission. Dispersion is introduced by the dependence of electrical path length on the local radius of curvature within the bend. This dispersion increases the risetime and broadens the pulse width of the transmitted signal, degrading system bandwidth.

In several papers, [3, 4, 5, 6, 7, and 8], Dr. Carl E. Baum has described an approach to address the bend dispersion problem. A conventional transmission line is filled with a *homogeneous* dielectric material, sometimes air, or is evacuated. Dr. Baum proposed compensation of a transmission line bend by a purely dielectric lens, characterized by an *inhomogeneous*, frequency-independent, isotropic permittivity. If the index of refraction of the lens varies inversely with the radius of curvature, then the optical path length and pulse transit time through the bend become independent of the radius. Dr. Baum has coined the term, "cylindrically inhomogeneous dielectric," or CID, for such a dielectric medium [9]. He has also proved that a transmission line bend compensated by a CID lens supports TEM waves.

We previously summarized the theory behind this approach to dispersion reduction and presented our hardware implementation of a strip line bend approximately compensated by five coarsely graded layers of dielectric materials having various uniform refractive indices [1 and 2]. That 90° bend, shown in Figure 1, achieved a 70 ps reduction in the risetime of a transmitted voltage step, when compared with an identical air-filled line. We ultimately concluded that the performance of the strip line was primarily limited by propagation of fringe fields ahead of and behind the main pulse.

Here, we apply lessons learned in the earlier strip line work to square coaxial hardware, the use of which eliminates troublesome fringe fields. We designed a constant-impedance, electrically large, square coaxial test set for use in comparing impulse propagation through both straight and curved transmission line sections. Although our design approach for a layered co
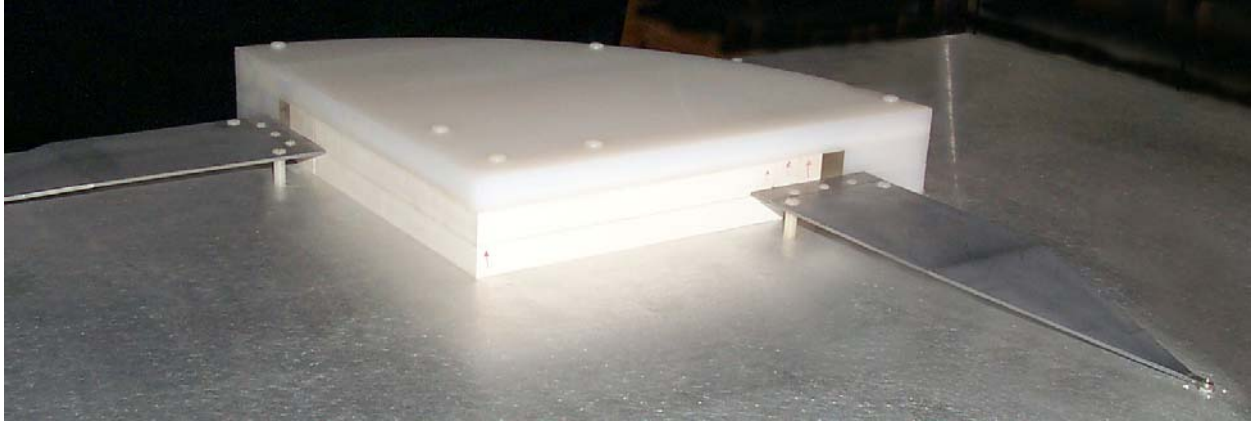
Figure 1.   Strip transmission line bend approximately compensated by five uniform dielectric layers. Dielectric constants vary from 2.3 to 4.4. The strip width is 6.35 cm (2.5"), and has an inner radius of curvature of 12.95 cm (5.1").

axial bend employed a manual heuristic algorithm, we subsequently performed a global optimization, which demonstrated that our design was very nearly optimal. To investigate a potentially inexpensive compensation approach, based on bends partially filled with dielectric material, we also designed wedge-shaped uniform dielectric fillers for the bend hardware. To guide all our designs, we employed a finite element-based impedance model of the transmission line cross section, which we derived to handle both straight transmission lines and bends with azimuthal symmetry [10].

In the following sections, we present both our coaxial hardware designs and observations of UWB impulse propagation through them. In contrast to the earlier layered strip line result, compensation of a coaxial bend by a layered dielectric dramatically improved impulse transmission through the bend.

2.   Design of a Dielectric Laminate to Compensate a Coaxial Transmission Line Bend

We began the process of designing a transmission line bend approximately compensated by graded layers of dielectric material by assuming a transmission line size and a maximum radius of curvature for a 90° bend. To simplify manufacture of the layered dielectric material, we chose a square cross section, which we assumed to be 5.08 cm (2") on each side. For consistency with an earlier design approach, we chose 14.68 cm (5.781") as the outer radius of curvature. With these choices, the centerline path length of the bend was 19.08 cm (7.51").

Next, we specified a performance goal for use in assessing the need for bend compensation. Our criterion was that the signal transit time through the bend should not vary by more than about 100 ps. The transit time at any radius is

$$\tau = \left(\Delta\phi/c\right)\Psi n \;=\; \left(\Delta\phi/c\right)\Psi\sqrt{\varepsilon_r} \tag{1}$$

where $\Delta\phi$ is the bend angle in radians, c is the speed of light, Ψ is the local radius of curvature, and n, the local index of refraction, is the square root of the relative dielectric constant, ε_r. For an uncompensated bend, the difference in transit time between the inner and outer radii of curvature is completely determined by the width of the bend and by the (constant) index of refraction. For an air-filled, 5.08 cm (2") wide, 90° bend, that time difference is 266 ps. It increases linearly with the index of refraction. Since the 100 ps limit is exceeded for the proposed bend, even in air, compensation is required.

To specify the design of a compensating dielectric laminate, we needed to identify dielectric materials and their properties. We selected a series of adjusted dielectric constant materials produced by Cuming Microwave Corporation, and known as C-Stock AK-500. These are plastics based on a polybutyldiene resin and loaded with varying quantities of titanium dioxide. They can be produced at half-integer increments of the dielectric constant from 3.0 to 10.0. Although the materials can be readily machined with sharp carbide tools, they are somewhat brittle, especially at the higher dielectric constants. The manufacturer recommended extreme care if layers thinner than about 0.64 cm (0.25") were to be machined. For this reason, we chose to avoid layers thinner than this limit. If all layers were of this minimal thickness, eight would be required to fill the radial extent of the bend. Since manufacturing cost increases with layer count,

we sought to use the minimum number of layers capable of meeting our assumed 100 ps transit time variation limit.

In a layered bend, there are two sources of transit time variation. Across the width of each layer, the transit time varies linearly, because the dielectric constant is uniform, while the radius of curvature changes. Across adjacent layers, the transit time changes abruptly, because the dielectric constant is discontinuous at the layer interface. In designing the bend, we applied the same $(\Delta\tau)_{max} = 100$ ps limit to both sources of transit time variation.

Finally, we sought a design in which the laminate of uniform dielectric layers would closely approximate the inverse square relationship between the dielectric constant and radius of curvature that characterizes a CID medium. To this end, we attempted to place the midpoint of each layer as close as possible to the correct radius for the dielectric constant of the material comprising that layer.

The following algorithm addresses layer definition subject to the goals and constraints identified above. Since higher indices of refraction dictate smaller layer widths to satisfy a given transit time variation limit, we prefer a set of materials comprising the lowest possible indices of refraction. Hence, we begin the layer definition process at the maximum radius of curvature with the material having the lowest dielectric constant. For the outermost layer, we use the maximum layer width consistent with the $(\Delta\tau)_{max} = 100$ ps limit. This is found from (1) as

$$(\Delta\Psi)_{max} = \frac{2c(\Delta\tau)_{max}}{\pi n} = \frac{2c(\Delta\tau)_{max}}{\pi\sqrt{\varepsilon_r}} \tag{2}$$

Next, we relate the design to the ideal dielectric constant profile by asserting that the ideal profile must pass through the midpoint, Ψ_{mp}, of this outermost layer. This allows us to estimate the radius at which the relative dielectric constant reaches unity as

$$\Psi_{max} = \Psi_{mp}\sqrt{\varepsilon_r} \tag{3}$$

For each subsequent layer, we calculate the maximum permissible dielectric constant, from (1) as

$$\varepsilon_{r,max} = \left(\frac{2c\Delta\tau}{\pi\,\Psi} + \sqrt{\varepsilon_{r,previous}} \right)^2 \tag{4}$$

Then, we choose the material with the largest dielectric constant not exceeding $\varepsilon_{r,max}$. If no such material exists, the time variation constraint at the layer interface cannot be satisfied. After selecting a material for the new layer, we calculate the maximum layer width from (2), and a tentative midpoint from

$$\Psi_{mp} = \Psi_{max}/\sqrt{\varepsilon_r} \tag{5}$$

The tentative width of the layer is $\Delta\Psi = 2\left(\Psi_{outer} - \Psi_{mp}\right)$. If this width exceeds $\left(\Delta\Psi\right)_{max}$ for the layer, we use $\Delta\Psi = \left(\Delta\Psi\right)_{max}$. If it is less than $\left(\Delta\Psi\right)_{min} = 0.64$ cm (0.25"), we use $\Delta\Psi = \left(\Delta\Psi\right)_{min}$. The inner radius of curvature of the layer is $\Psi_{inner} = \Psi_{outer} - \Delta\Psi$. If the residual between Ψ_{inner} and the innermost bend radius exceeds $\left(\Delta\Psi\right)_{min}$, then there is adequate space for yet another layer. If the residual is less than $\left(\Delta\Psi\right)_{min}$, some adjustments of layer boundaries are required to complete the design. We either decrease some layer widths to increase the residual, up to at least $\left(\Delta\Psi\right)_{min}$, making room for a final layer; or we increase some existing layer widths to absorb the residual.

The algorithm described above leads to a preliminary layer design. Since enforcement of the constraints and adjustments of layer boundaries generally displace layer midpoints from the assumed ideal dielectric constant profile, a new Ψ_{max} is obtained by averaging $\Psi_{max} = \Psi_{mp}\sqrt{\varepsilon_r}$ over all layers. Then we use (5) to recalculate ideal layer midpoints. Finally, we adjust layer boundaries, as possible, to move the layer midpoints in the direction of the ideal locations.

Application of the foregoing process led to a six-layer design employing materials with dielectric constants of 3.0, 3.5, 4.0, 4.5, 5.0, and 6.0. The layer-thickness-weighted average dielectric constant is 4.1. As the plots in Figure 2 demonstrate, the result represents a good approximation to a CID profile with $\Psi_{max} = 24.475$ cm (9.636"). The target maximum variation of 100 ps from minimum to maximum transit time is exceeded only at the interface between the innermost two layers. In contrast, an uncompensated bend, filled with a material having a dielectric constant of 4.1, would exhibit more than five times the 100 ps limit between inner and outer radii of curvature. In the plot of transit time variation, note that the definition of $\Delta\tau$ is different from that used in describing the design algorithm. There, it was the absolute value of a variation in transit

Dielectric Constant Profile for a Coaxial Bend with Ψ_{max} = 9.636in.
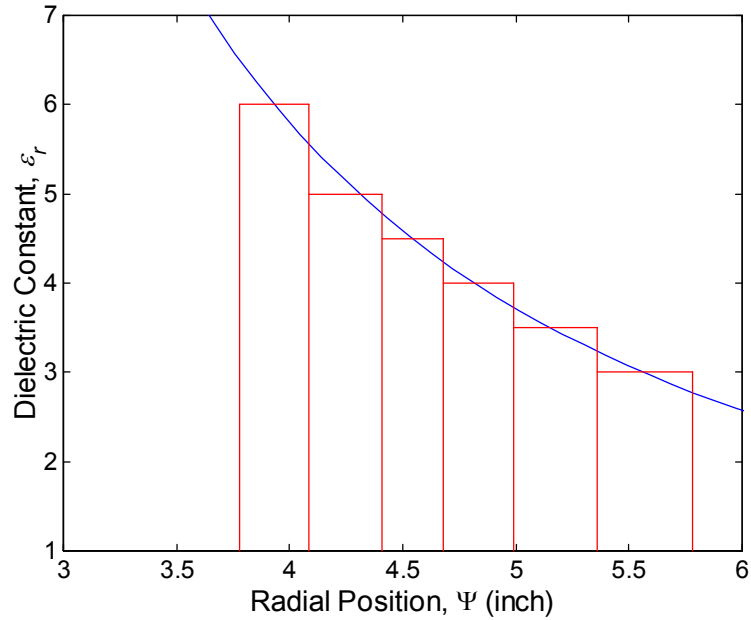
Transit Time Variation for a Layered Coaxial Bend, Ψ_{max} = 9.636in.
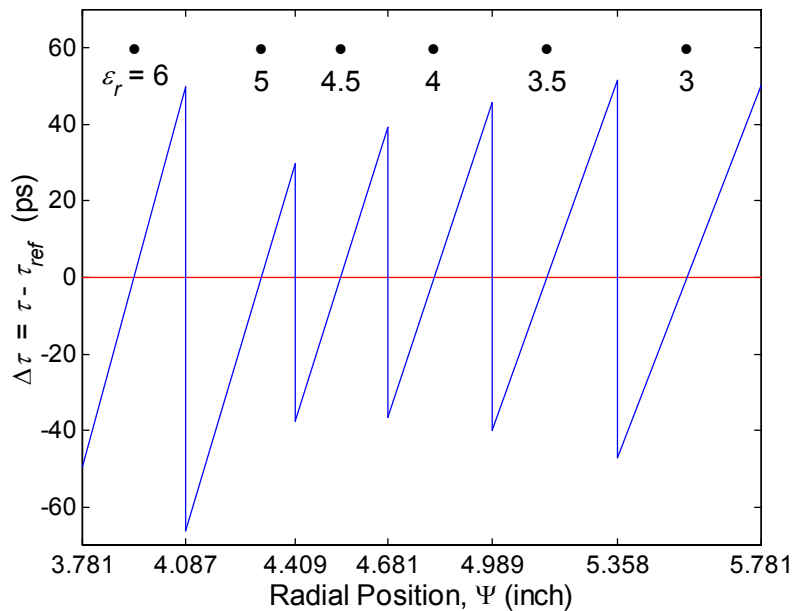
Figure 2. Dielectric laminate design for use with a coaxial bend. The top plot shows the inverse square profile for an ideally graded bend with an overlay of the histogram representing the layered approximation. The lower plot shows the predicted variation of the transit time from the ideal, across the radial extent of the bend. The bullets indicate the radial positions at which the ideal dielectric constant profile intersects each layer. Dimensions are inches.

times between different locations or different materials. Here, it is defined as the radius-dependent difference between a predicted transit time and the constant transit time through an ideal, 90° CID bend. Thus, in the transit time variation plot, (1) has been evaluated at Ψ and Ψ_{max} to obtain

$$\Delta\tau \equiv \tau - \tau_{ref} = \left(\Psi\sqrt{\varepsilon_r} - \Psi_{max}\right)\Delta\phi/c \tag{6}$$

where $\Delta\phi = \pi/2$ for the 90° bend.

The heuristic process we have used here to design the dielectric laminate works well, but is tedious to apply, and provides no indication as to whether the result is anywhere near optimal. In Appendix A, we derive an objective function for use in obtaining a globally optimal design, subject to all relevant constraints. That function is the root-mean-square of (6), over all dielectric layers. Specifically, for an N_l-layer bend, we use

$$\left(\Delta\tau\right)_{rms} = \left\{\frac{1}{N_l}\sum_{i=1}^{N_l}\frac{\int_{\Psi_{i-1}}^{\Psi_i}\left(\Delta\tau\right)_i^2 \, d\Psi}{\Psi_i - \Psi_{i-1}}\right\}^{1/2} \tag{7}$$

The optimal set of dielectric constants and layer-bounding radii of curvature, is that which minimizes (7), subject to all applicable constraints. The resulting globally optimal set is nearly identical to the one produced by the heuristic algorithm. The associated minimum value of $\left(\Delta\tau\right)_{rms}$ is 27 ps.

3.   Integration of the Dielectric Laminate with a Transmission Line Bend Test Fixture

We integrated the dielectric laminate with a 50 Ω square coaxial TEM transmission line bend test fixture. To minimize reflections, we required that the bend and its interfaces have identical conductor sizes in addition to having the same nominal impedance. Since the layer-thickness-weighted average dielectric constant within the bend is 4.1, we chose dielectric constant 4.0 material to fill the straight (tapered) sections interfacing to the bend. There is a parametric expression available for the impedance of a uniform straight square coax with cylindrical center conductor [11]. With a dielectric constant of 4.0, it predicts 50 Ω, when the length of the side of the outer conductor is five times the diameter of the inner conductor. Since the outer conductor must be 5.08 cm (2.0") on each side, we selected 1.016 cm (0.4") as the diameter of the inner conductor.

To predict the impedance of the layered transmission line bend, we modeled the cross section using finite elements and calculated the impedance as described in [10]. There we proved that the characteristic impedance could be found (approximately) from

$$Z_C = Z_0 \left(\frac{\Psi_{max}}{\mathbf{U}^\mathbf{T} \mathbf{S} \mathbf{U}} \right) \qquad (8)$$

Here, Z_0 is the impedance of free space, $\mathbf{T}$ is the vector transpose operator, and $\mathbf{S}$ and $\mathbf{U}$ are, respectively, the finite element matrix and solution vector for the two-dimensional potential equation for a rotationally symmetric geometry,

$$\nabla \cdot \left(\Psi \, \varepsilon_r \nabla u \right) = 0$$
$$\text{where } \nabla \equiv \left(\frac{\partial}{\partial \Psi} \hat{\Psi} + \frac{\partial}{\partial z} \hat{z} \right) \qquad (9)$$

The electrical potential, u, is a function only of Ψ and z, and $\hat{\Psi}$ and $\hat{z}$ are unit vectors. For a layered bend, (8) is valid to the extent that the layers represent a good approximation of the ideal continuously graded bend. The model result was $Z_C = 49.8$ Ω. The cross section of the layered bend model, showing the position of the center conductor, is shown in Figure 3. A top view of the bend layers is shown in Figure 4.

Layered Coaxial Bend, $\langle\varepsilon_r\rangle \approx 4.1$, $Z \approx 50\Omega$, $\Psi_{max} = 9.636$in.
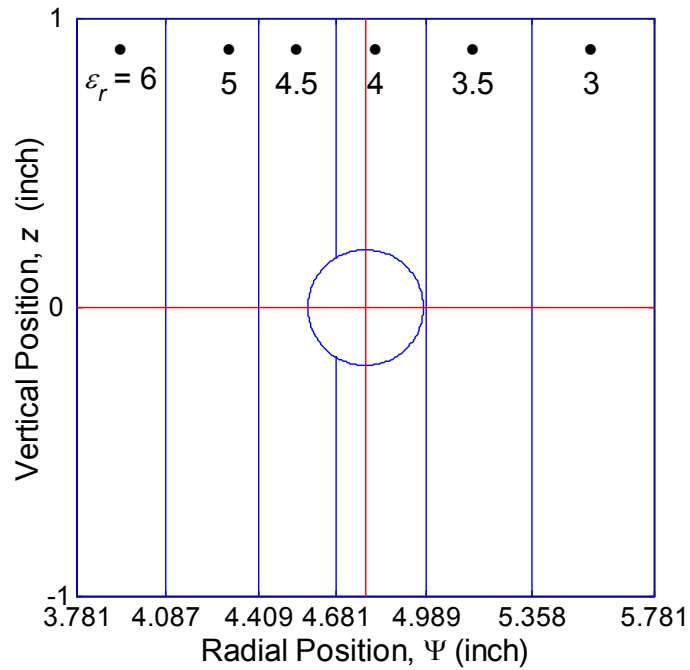
Figure 3. Geometry of the finite element model of the cross section of the layered bend. The center conductor diameter is 1.016 cm (0.4"). Dimensions are inches.

Layered Coaxial Bend, $\langle\varepsilon_r\rangle \approx 4.1$, $Z \approx 50\Omega$, $\Psi_{max} = 9.636$in.
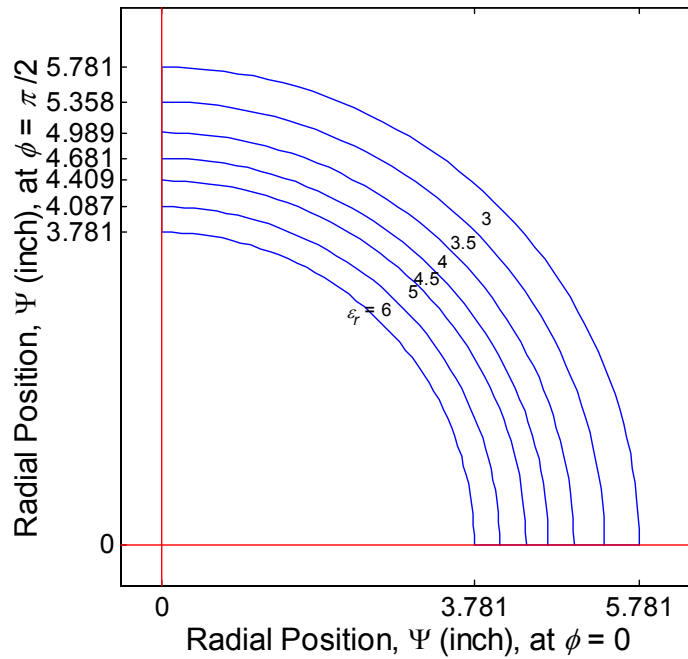
Figure 4. Top view of the layered bend design. Dimensions are inches.

In addition to the coaxial bend test section, we also designed a pair of square pyramidal taper sections to provide a constant impedance transition between the 5.08 cm (2") square coax and a standard 50 Ω N-type female connector. A solid CAD model of the taper section is shown in Figure 5 The outer conductor of the taper shrinks from 5.08 cm (2") square to 0.975 cm (0.384") square over a 15.24 cm (6") length. At the same time, the center conductor shrinks from a diameter of 1.016 cm (0.4") to one of only 0.196 cm (0.077"). At the transition to the N-type connector, the outer conductor cross section changes from square to circular, with a diameter of 0.975 cm (0.384"). At the same transition point, the diameter of the inner conductor jumps to 0.305 cm (0.12"), as the dielectric constant of the surrounding medium changes from 4.0 in the taper to about 2.0 in the N-type connector.
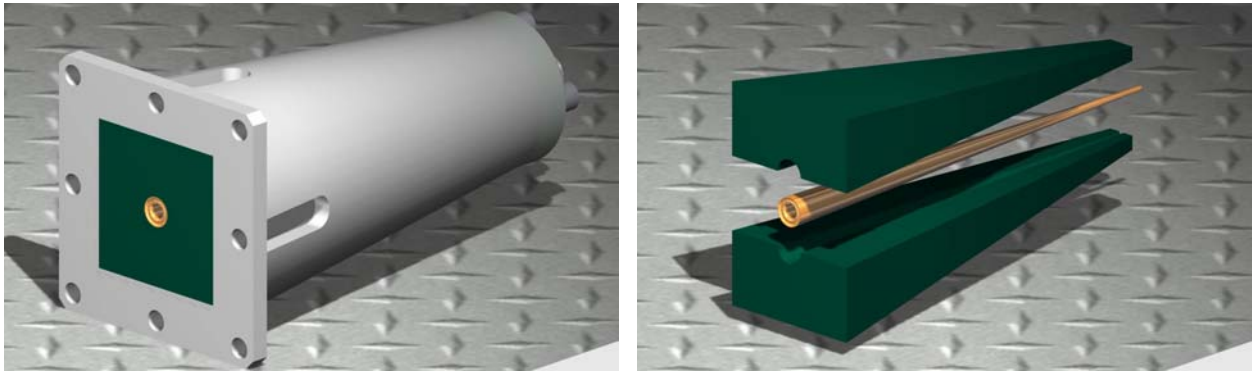
Figure 5. Tapered coaxial transmission line section CAD model. The taper provides a 50 Ω transition between the square coaxial geometry and an N-type cable connector. The image on the left is an assembled taper; on the right is an exploded view of the dielectric filler and center conductor.

The complete transmission line bend assembly, consisting of a pair of tapered sections and a 90° bend, is depicted in Figure 6. The diagram in the upper portion of the figure is a z-plane cross section at the fixture centerline. The layered dielectric lens fills the bend. The lower portion of the figure is a photograph of the fully assembled test fixture.
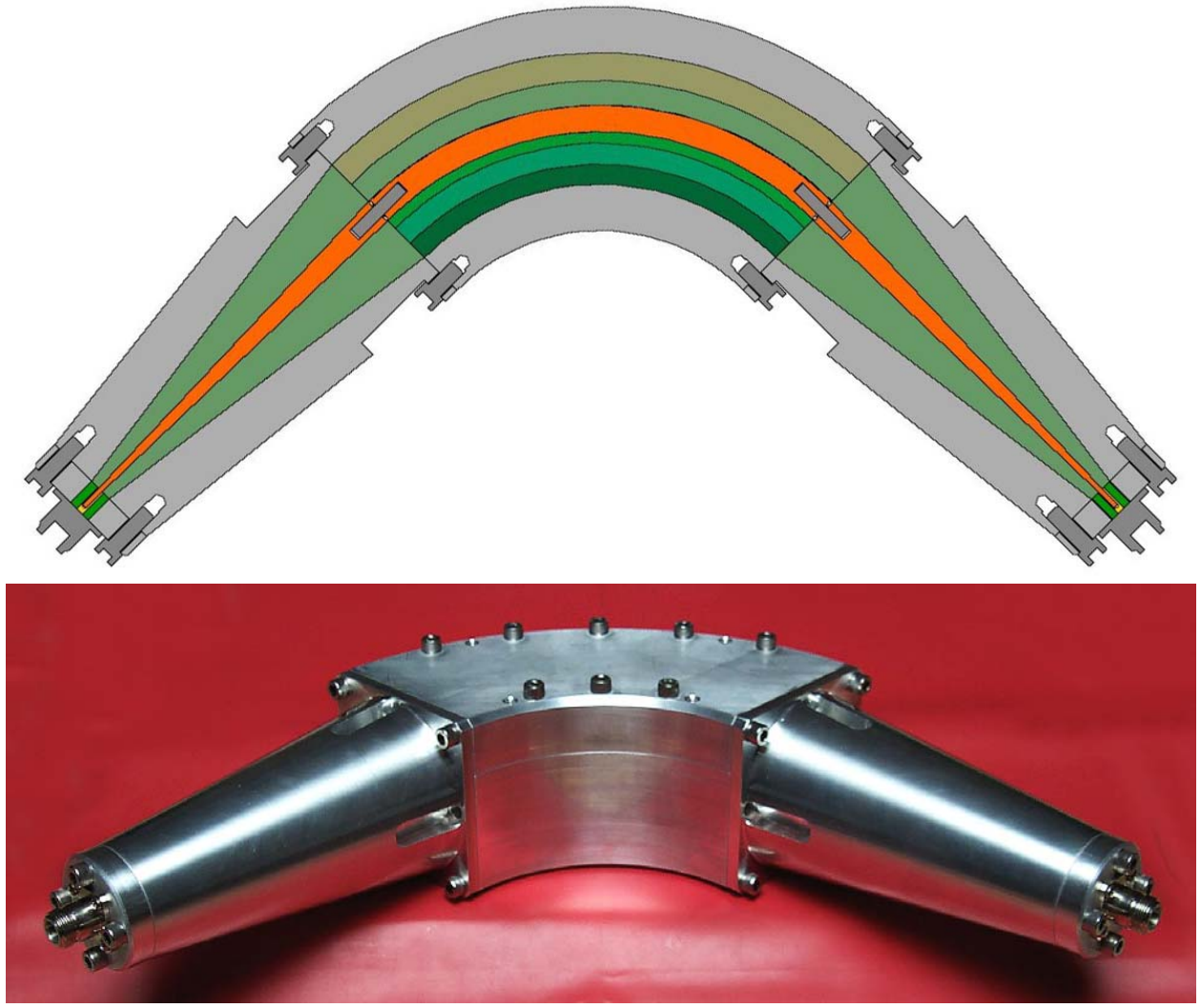
Figure 6.   Square coaxial transmission line test fixture with 90° bend. The CAD drawing is a *z*-plane cut through the test fixture centerline. The photo is of the fully assembled test fixture.

4. Other Test Articles

In addition to the laminated dielectric bend, five other dielectric samples were tested by impulse propagation in the square coaxial fixture. First, material with a dielectric constant of 4.0 was measured within a straight 5.08 cm (2") square coax transmission line section, having the same length as the centerline of the coaxial bend section, 19.08 cm (7.51"). The purpose of this measurement was to obtain a "best case" for comparison with compensated bend results. A perfectly compensated bend would be expected to perform as well as a straight section. A bend filled with the same dielectric material provided a "worst case" example.

The remaining three samples (actually one sample at three different stages of machining) tested the concept using a shaped partial dielectric fill to compensate a coaxial bend. This attempt was motivated by the hope of avoiding the large machining cost of the laminated bend method. The rationale for this approach is rooted in the concept of a parallel-plate capacitor in which fringe fields can be neglected and the gap between the plates is only partially filled with a dielectric. In that case, one can calculate the fraction of the gap, which must be filled to produce any specified effective dielectric constant between 1.0 and the intrinsic relative dielectric constant of the fill material. Unfortunately, there are two expressions relating the fill fraction and the effective dielectric constant. One applies when the electric field is perpendicular to the dielectric-air interface; the other applies to the parallel case. As we have previously noted in [1], the expressions are

$$f_\perp = \frac{1 - \varepsilon_{r,eff}^{-1}}{1 - \varepsilon_r^{-1}} \quad \text{and} \quad f_7 = \frac{\varepsilon_{r,eff} - 1}{\varepsilon_r - 1} \tag{10}$$

To obtain fill fractions as a function of radius of curvature, we let $\varepsilon_{r,eff} = (\Psi_{max}/\Psi)^2$, and obtain the pair of results shown in Figure 7, for $\Psi_{max} = 24.475$ cm (9.636") and $\varepsilon_r = 6.0$. To convert the fill fractions to a shaped partial dielectric fill for the coaxial bend, we associate the fill fractions with the portion of the vertical extent of the bend that is filled with dielectric. To obtain a symmetric shape, we distribute half of the dielectric above and half below the centerline. Figure 8 shows results for both parallel and perpendicular calculations. Also shown, in the upper half of the figure, is a plane surface "average" of the parallel and perpendicular results. For want of a better choice, we use this "average" result for our "Blunt Wedge" sample. A finite element

13

Fill Fractions with ε_r = 6 for a Coaxial Bend with Ψ_{max} = 9.636in.
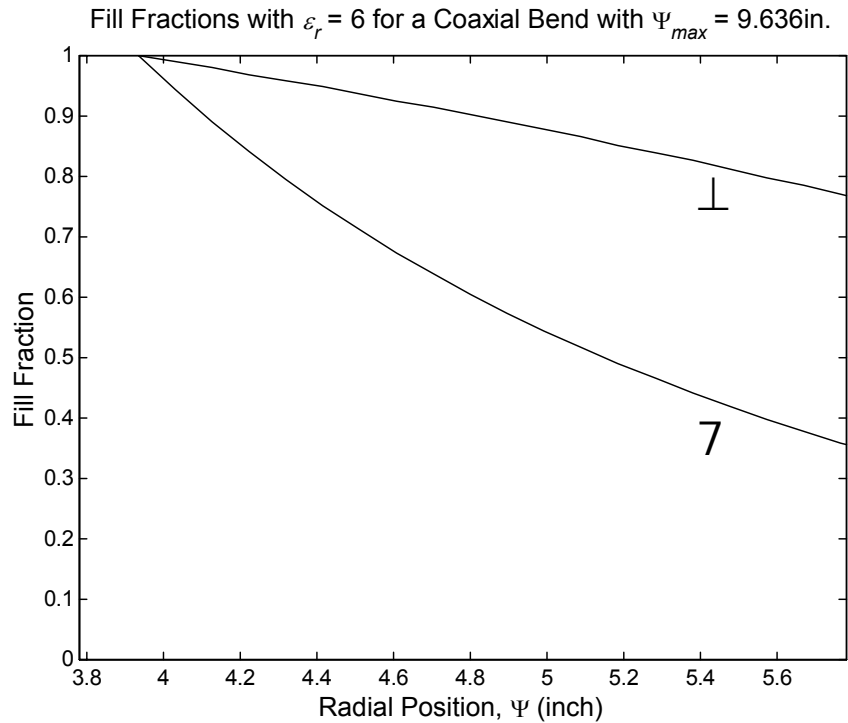
Figure 7. Dielectric fill fractions intended to produce an effective dielectric constant that varies inversely with the square of the radius of curvature. The dotted (upper) curve is for the perpendicular calculation of fill fraction. The lower (dot-dash) curve is for the parallel calculation

model of this design yields an impedance of about 40 Ω. Since the impedance should be 50 Ω, the average effective dielectric constant must be too high. This result suggested another partial fill sample, one in which the angle of the wedge is cut to achieve a 50 Ω impedance. Although this implies the correct average for the effective dielectric constant, it says nothing about its radial profile. This model, identified as the "Sharp Wedge", is shown in the lower half of Figure 8. Photographs of the hardware are presented in Figure 9.

As the initial sample in this group of three, we measured a uniform bend with dielectric constant of 6.0 (another "worst case" example). This was the same dielectric material which was subsequently machined to form the blunt wedge and later the sharp wedge designs.

Partially Filled Coaxial Bend, ε_r = 6, $Z \approx 39.6\Omega$, Ψ_{max} = 9.636in.

Partially Filled Coaxial Bend, ε_r = 6, $Z \approx 49.8\Omega$, Ψ_{max} = 9.636in.
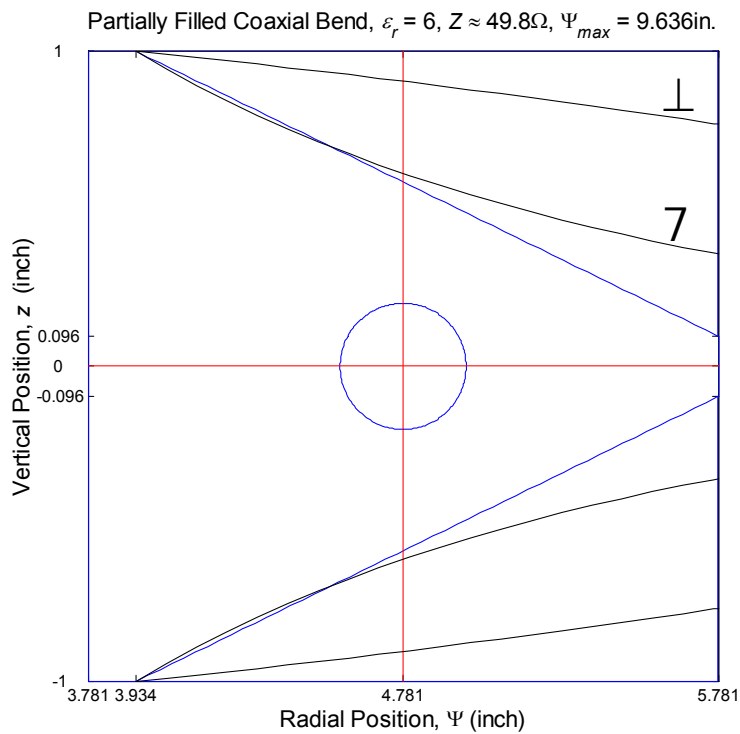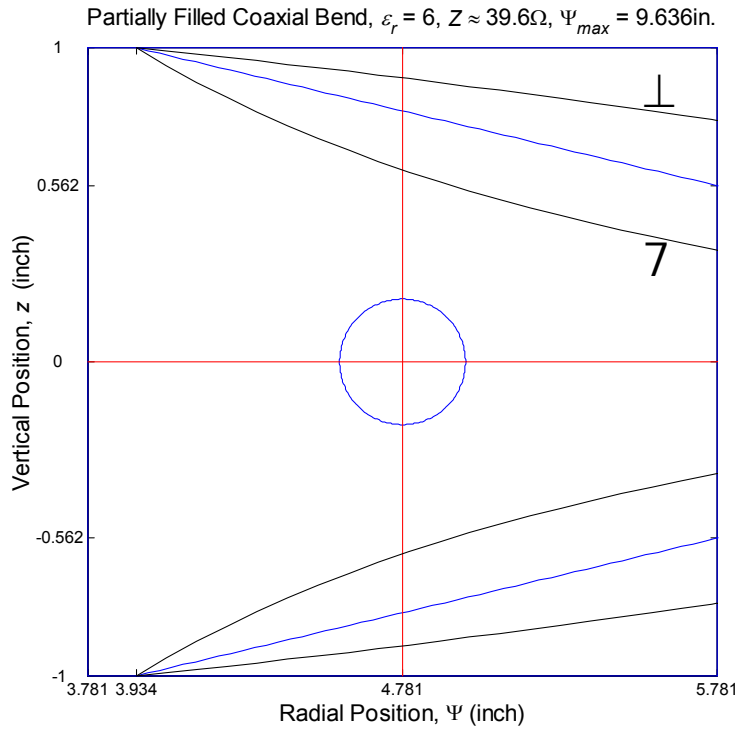
Figure 8.   Blunt (top) and sharp (bottom) wedge designs (straight, solid lines). Perpendicular and parallel fill fraction shapes are indicated by the broken line curves. Dimensions are inches.

15
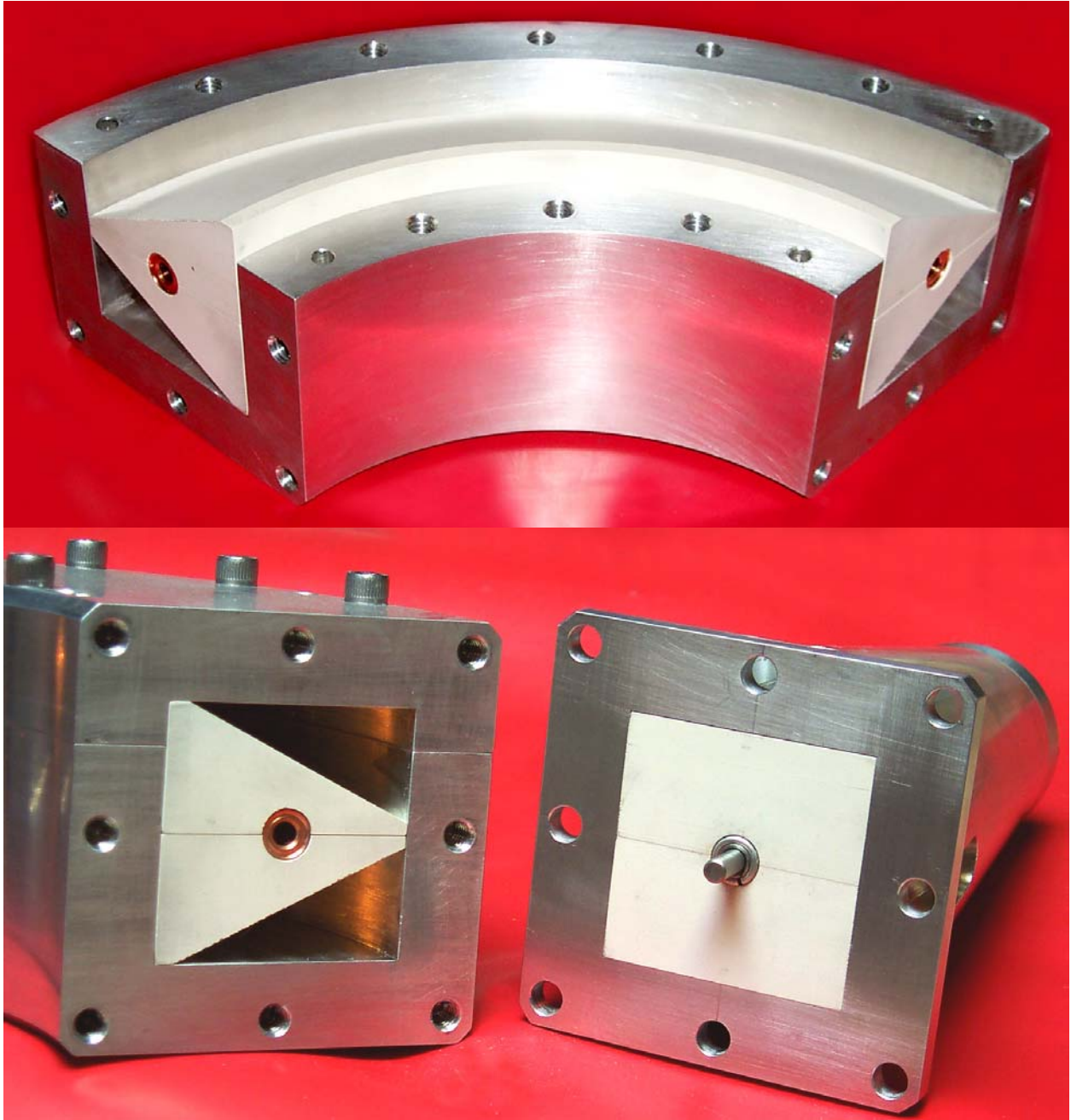
Figure 9.   Sharp wedge partial dielectric fill design. The upper photograph shows the partially assembled bend. The lower shows an end view of the wedge-bend assembly, along with one of the two mating taper sections. The dielectric constant of the wedge material is 6.0; that of the taper material is 4.0.

5.   Experimental Program

5.1   Equipment Setup and Signal Processing

The instrumentation and test fixture setup for the coaxial transmission line measurements is shown in Figure 10. The device under test (DUT) was either a 90° bend or straight section loaded with dielectric material. After propagation through the test fixture, the raw impulse response was detected by the SD-24 sampling head, and stored on the Tektronics 11801B oscilloscope. A cable correction measurement observed the PSPL 5210 output through the 61 cm Goretex cable. To obtain a system correction measurement, the DUT was removed and the two tapered sections were directly connected, as shown in Figure 11. Signal processing was used to isolate the response of the DUT by deconvolving the system response from the raw transmission data.[†] Impedance measurements employed the 0.25 voltage step of SD-24 operating in TDR mode, while a 50 Ω terminator replaced the PSPL 5210. Not shown in the setup diagram are a pair of N/SMA adapters, which interfaced the taper sections to the Goretex cables. These adapters are visible at the ends of the tapers in Figure 11.
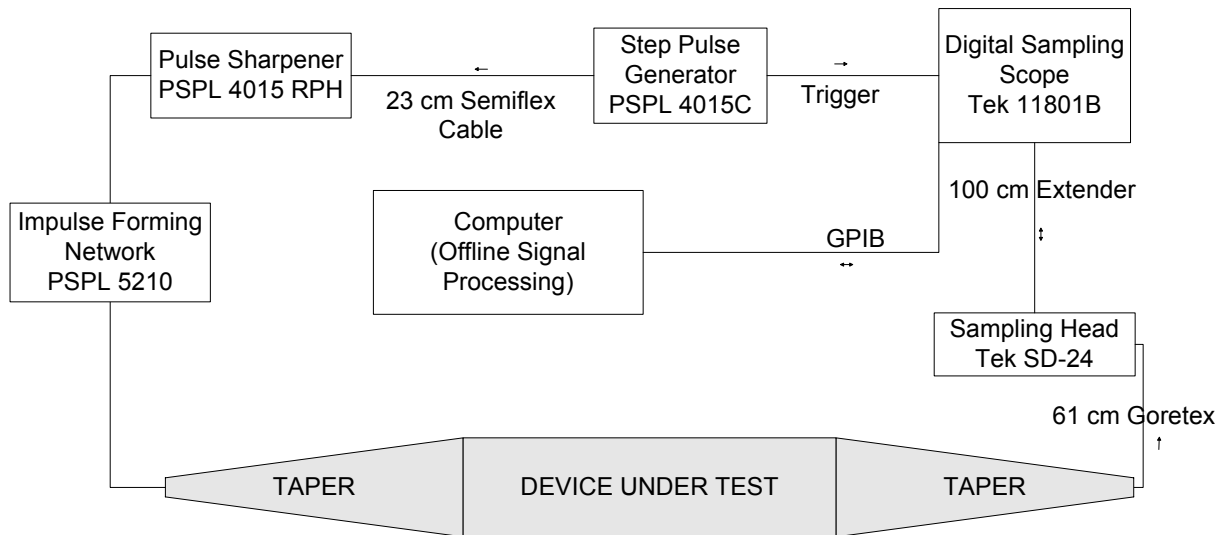
Figure 10. Equipment setup for coaxial transmission line measurements. The device under test (DUT) was either a 5.08 cm (2") square 90° coaxial bend or straight section loaded with a dielectric medium. Measurement waveforms were downloaded through the GPIB bus to a computer for offline signal processing.

[†] The cable response was never used independently in the signal processing. It is implicitly included within the system response.

Figure 11. Tapered coaxial transmission line transition sections configured for a system response correction measurement.

5.2   Measurements

Cable and system response measurements are presented in left and right columns, respectively, of Figure 12.[‡] The FWHM of the cable impulse response is 38 ps. The noise in its TDR at about 8 ns is caused by the N-type connector joining input and output cables. The FWHM of the impulse response for the pair of tapers, the system response, is 50 ps. In the TDR, the impedance increase at about 8 ns corresponds to the input connector. This is followed by a peak and downward ramp caused by a minor machining error in the taper angle. The peak at 10 ns represents the joint between the two tapers. At about 12.3 ns, we see the connector on the output taper. Note that the impedance of the output taper is flat, reflecting accurate machining of the taper angle.

An end view of the straight coaxial transmission line section is shown in Figure 13. Measurement data for this device are presented in Figure 14 (TDR), Figure 15 (raw impulse response), and Figure 16 (corrected impulse response). The TDR features at about 8 ns correspond to an N/SMA adapter and to the input N-type connector. The peak with the late-time ramp is the input taper. The small bump at about 12.8 ns is the interface to the output taper. Within the straight section, the impedance is 50.5 Ω. The features starting at about 15 ns are at the output N/SMA adapter. The FWHM of the raw time domain response of the straight section is 55 ps.

[‡] All figures mentioned in this discussion of TDR and impulse transmission measurements are grouped at the end of the section, beginning on page 20, and concluding on page 28.

The FWHM of the corrected time domain response is 40 ps. A 5th order modified Butterworth filter with a 15 GHz cutoff was used in deconvolving the system response from the raw data.

TDR and raw impulse transmission data for the coaxial bend filled or partially filled with the sundry uniform dielectric configurations are presented in Figure 17. None of these bend configurations is capable of preserving the impulse during transmission. In all cases, the impulse is transformed into a broad bipolar signal spanning an interval of approximately 500 ps.

An end view of the dielectric laminate-filled coaxial transmission line bend is shown in Figure 18. Measurement data for this device are presented in Figure 19 (TDR), Figure 20 (raw impulse response), and Figure 21 (corrected impulse response). The TDR features are very similar to those observed with the straight section of transmission line. Within the bend, the impedance is a flat 50.4 Ω. The FWHM of the raw time domain response of the bend is 70 ps, only 15 ps wider than that observed for the comparable straight section. The FWHM of corrected time domain response is 44 ps, only 4 ps wider than the corrected response for the straight section. Again, a 5th order modified Butterworth filter with a 15 GHz cutoff was used in deconvolving the system response from the raw data.
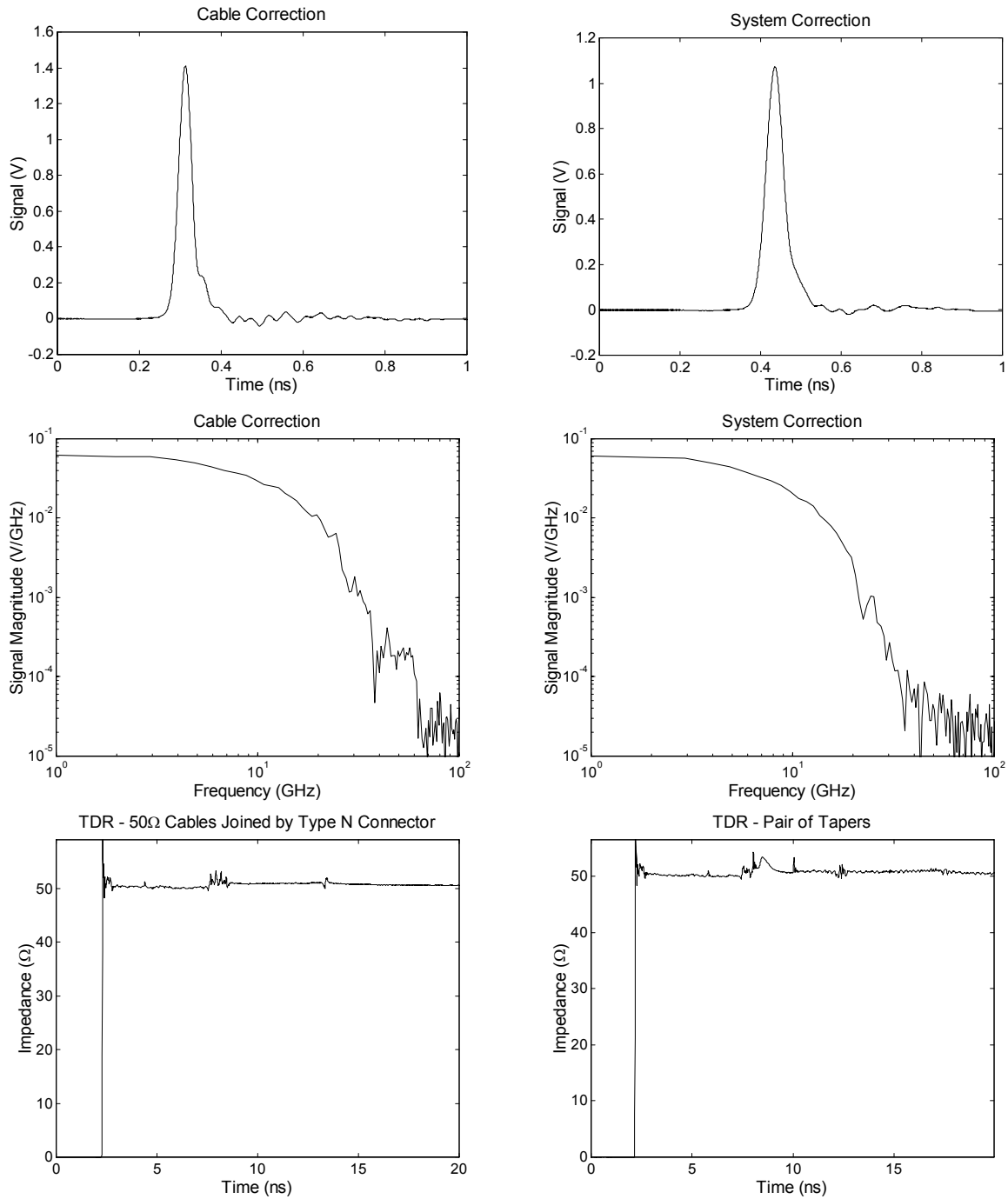
Figure 12. Cable and system impulse responses and TDR measurements. Plots of cable measurements are in the left column. System measurements are on the right.
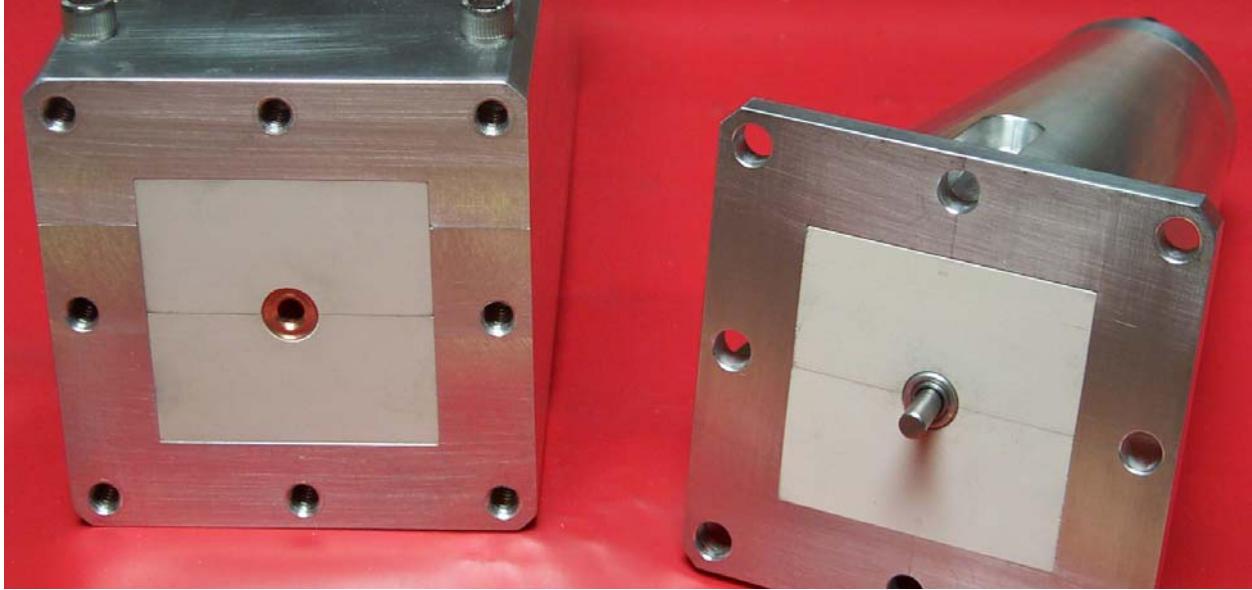
Figure 13. Straight section (left) shown with one of two mating taper sections (right).
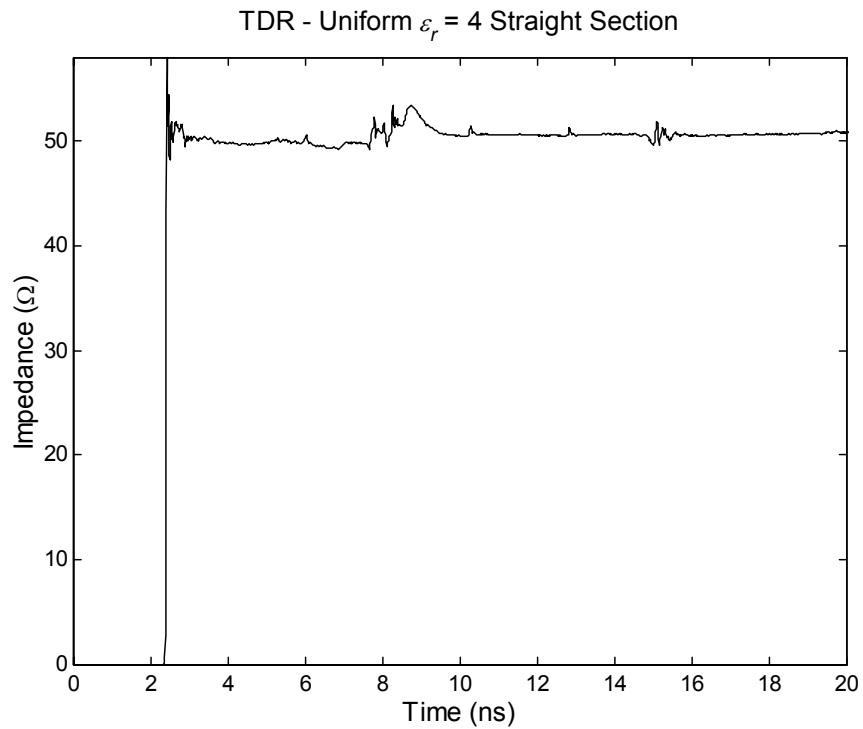
Figure 14. TDR of the straight section filled with a uniform $\varepsilon_r = 4$ dielectric. The small bump at 10.3 ns is the taper-to-straight section interface. The even smaller bump at about 12.8 ns is the interface to the output taper. Within the straight section, the impedance is 50.5 Ω.
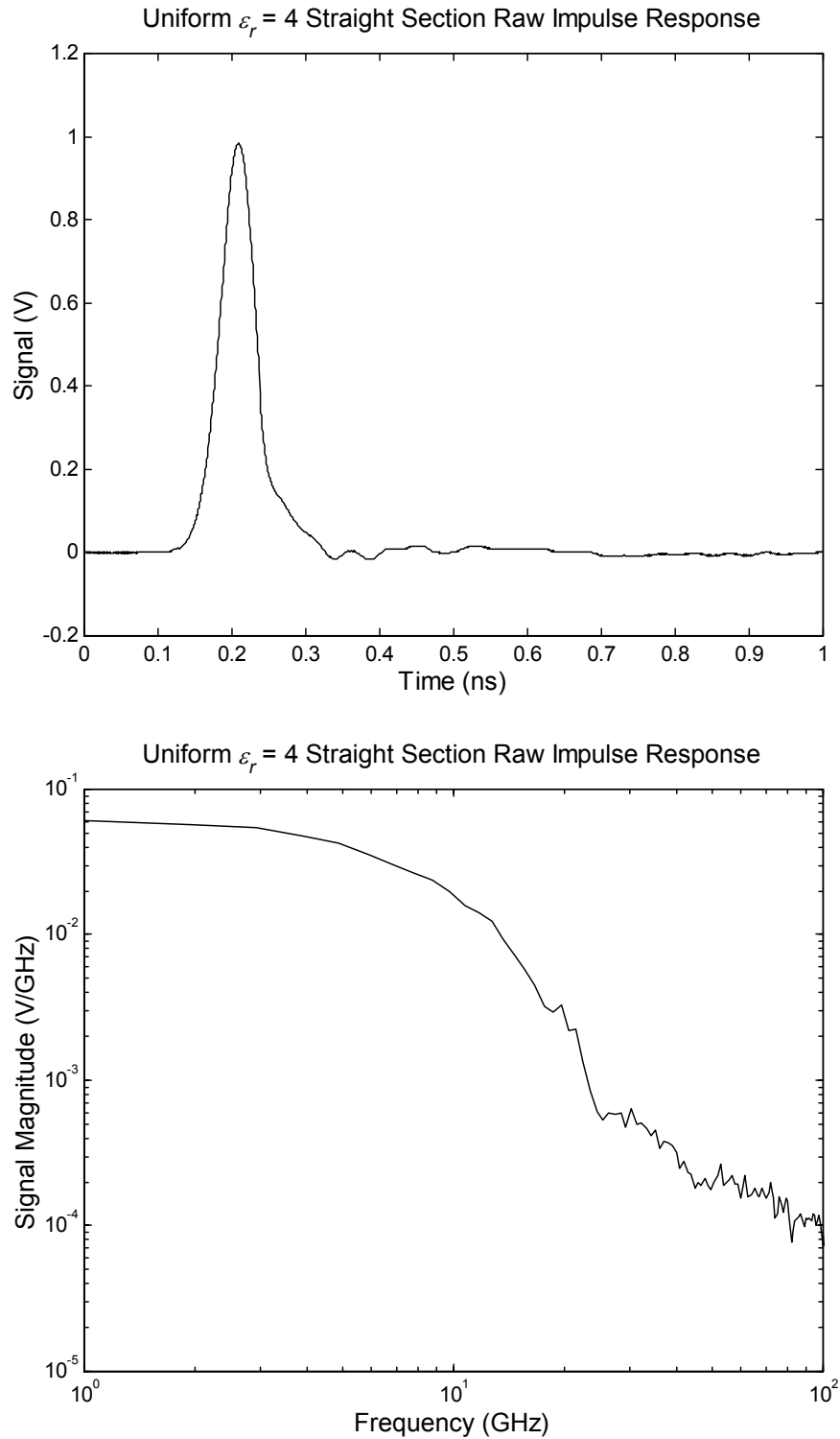
Figure 15. Raw impulse response for the 19.08 cm (7.51") straight section filled with a uniform $\varepsilon_r = 4$ dielectric. The FWHM of the time-domain peak is 55 ps.
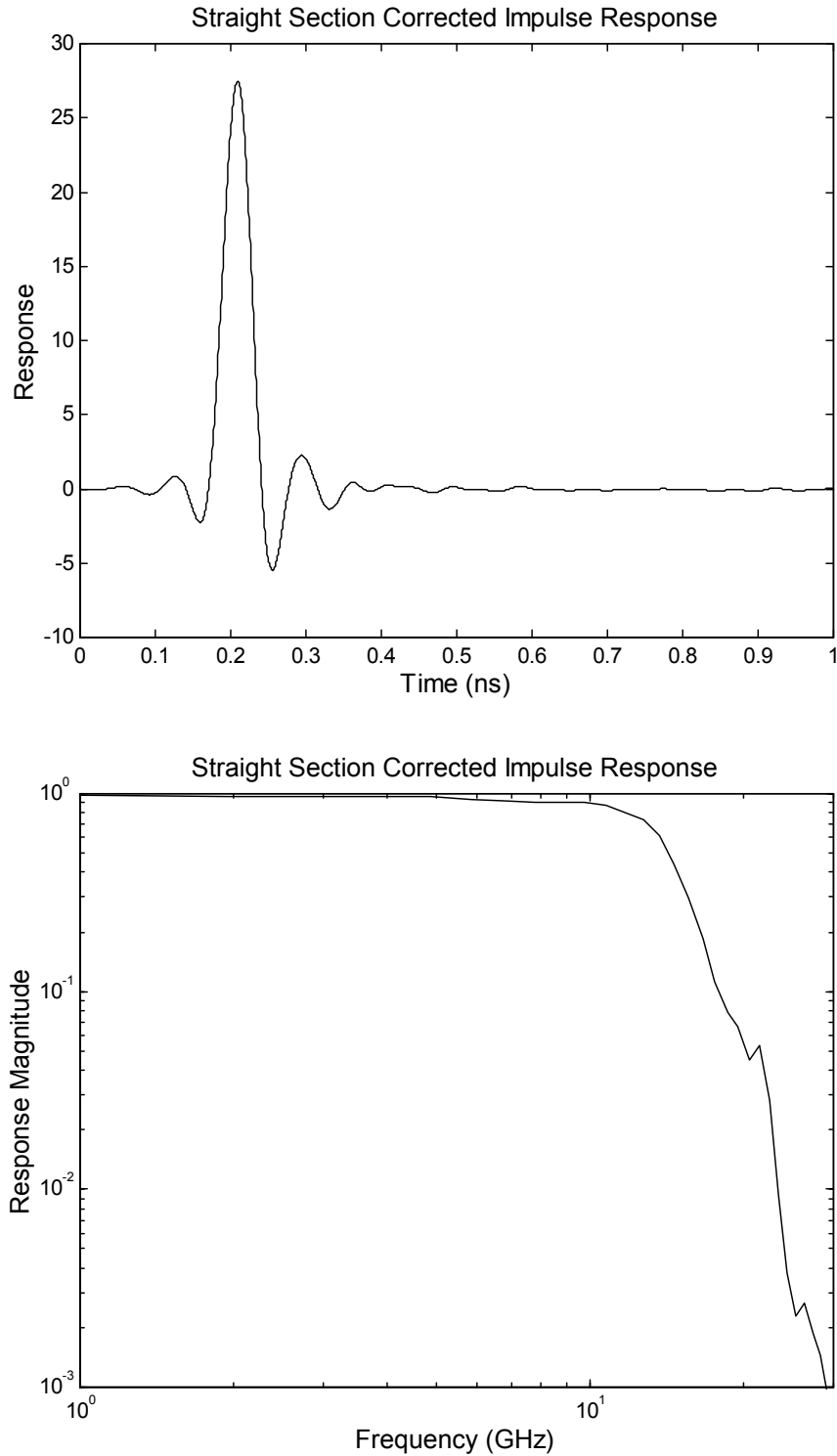
Figure 16. Corrected impulse response for the 19.08 cm (7.51") straight section filled with a uniform $\varepsilon_r = 4$ dielectric. The FWHM of the time-domain peak is 40 ps. A 5th order modified Butterworth filter with a 15 GHz cutoff was used in deconvolving the system response from the raw data.
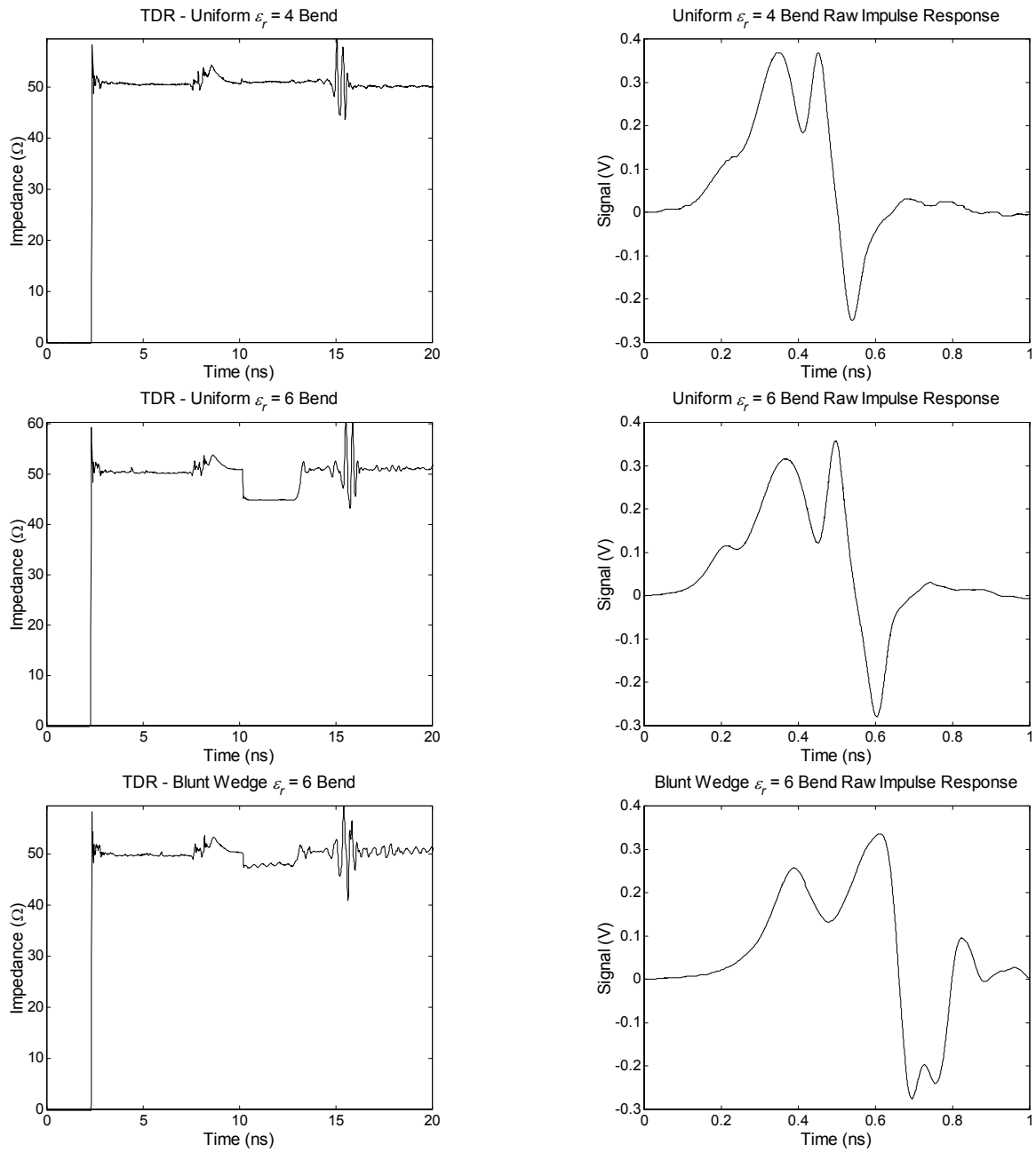
Figure 17. TDR and impulse response data for uniform and partially filled bends. Note the enhanced ringing at the output N/SMA adapter, and, for the wedges, within the bend itself. None of these bends is able to transmit a reasonable facsimile of an impulse.

TDR - Sharp Wedge ε_r = 6 Bend

Sharp Wedge ε_r = 6 Bend Raw Impulse Response

25
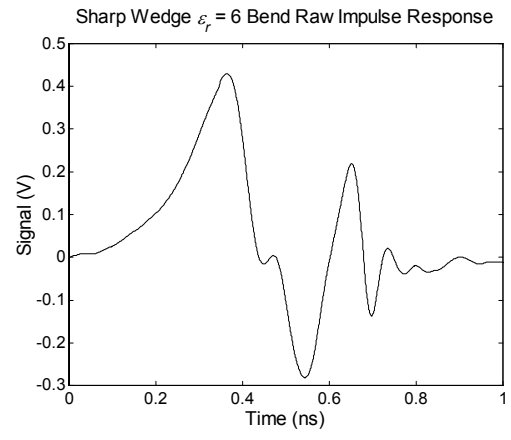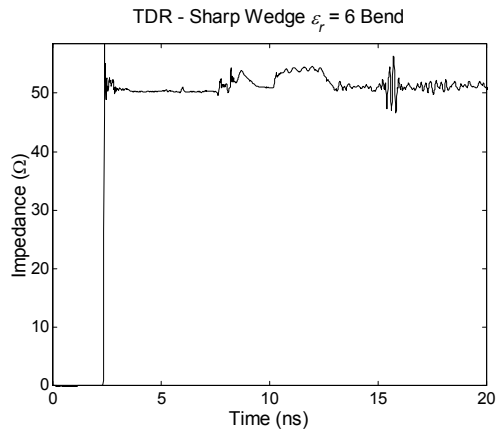
Figure 18. Layered dielectric bend (left), shown with one of two mating taper sections (right).
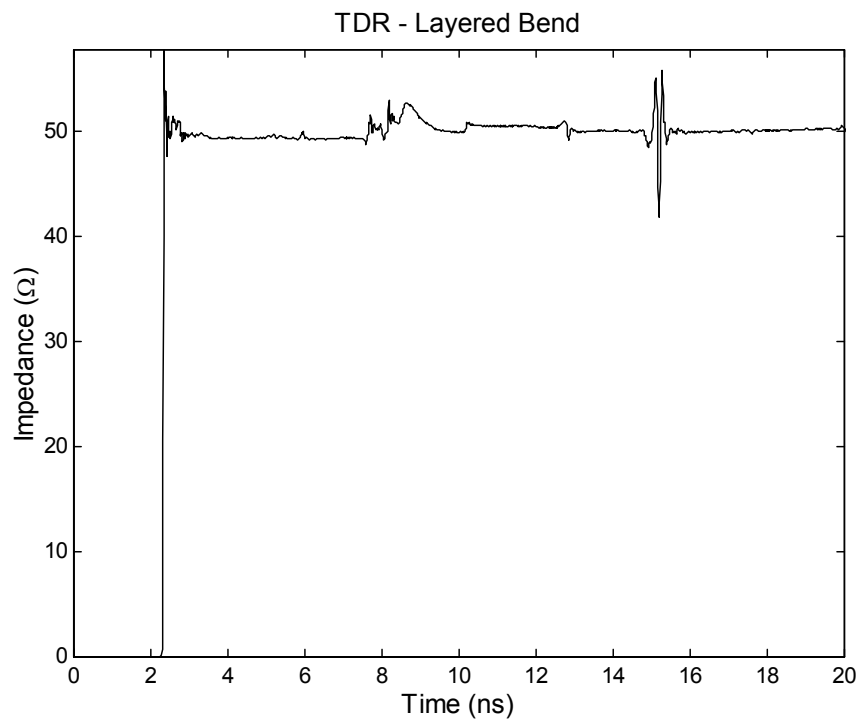
Figure 19. TDR of the six-layer dielectric laminate-filled bend. The small bump at 10.1 ns is the taper-to-bend interface. The other small bump at about 12.8 ns is the interface to the output taper. Within the bend, the impedance is a flat 50.4 Ω.
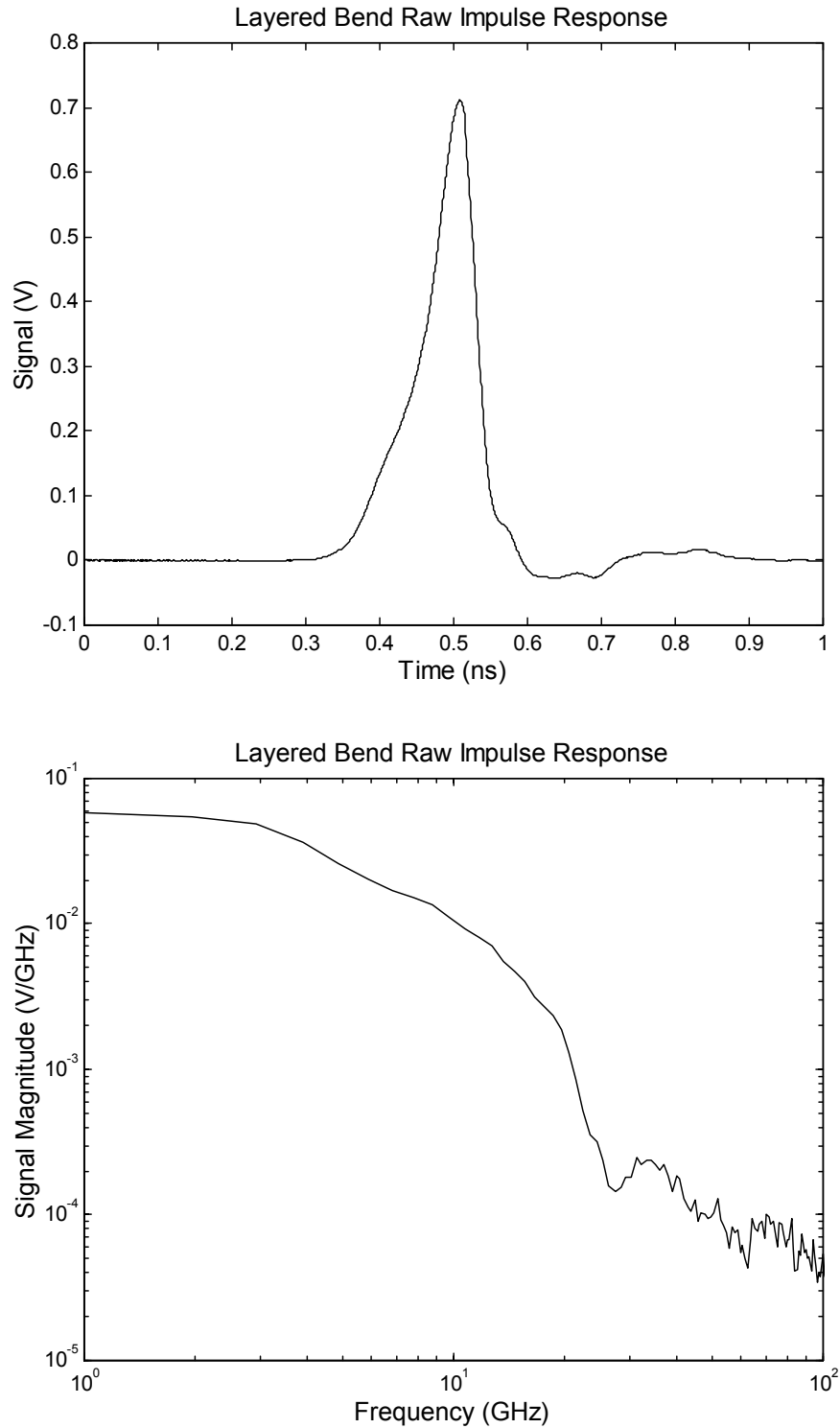
Figure 20. Raw impulse response for the six-layer laminated bend. The FWHM of the time-domain peak is 70 ps, only 15 ps wider than that observed for the comparable straight section of transmission line filled with a uniform dielectric.
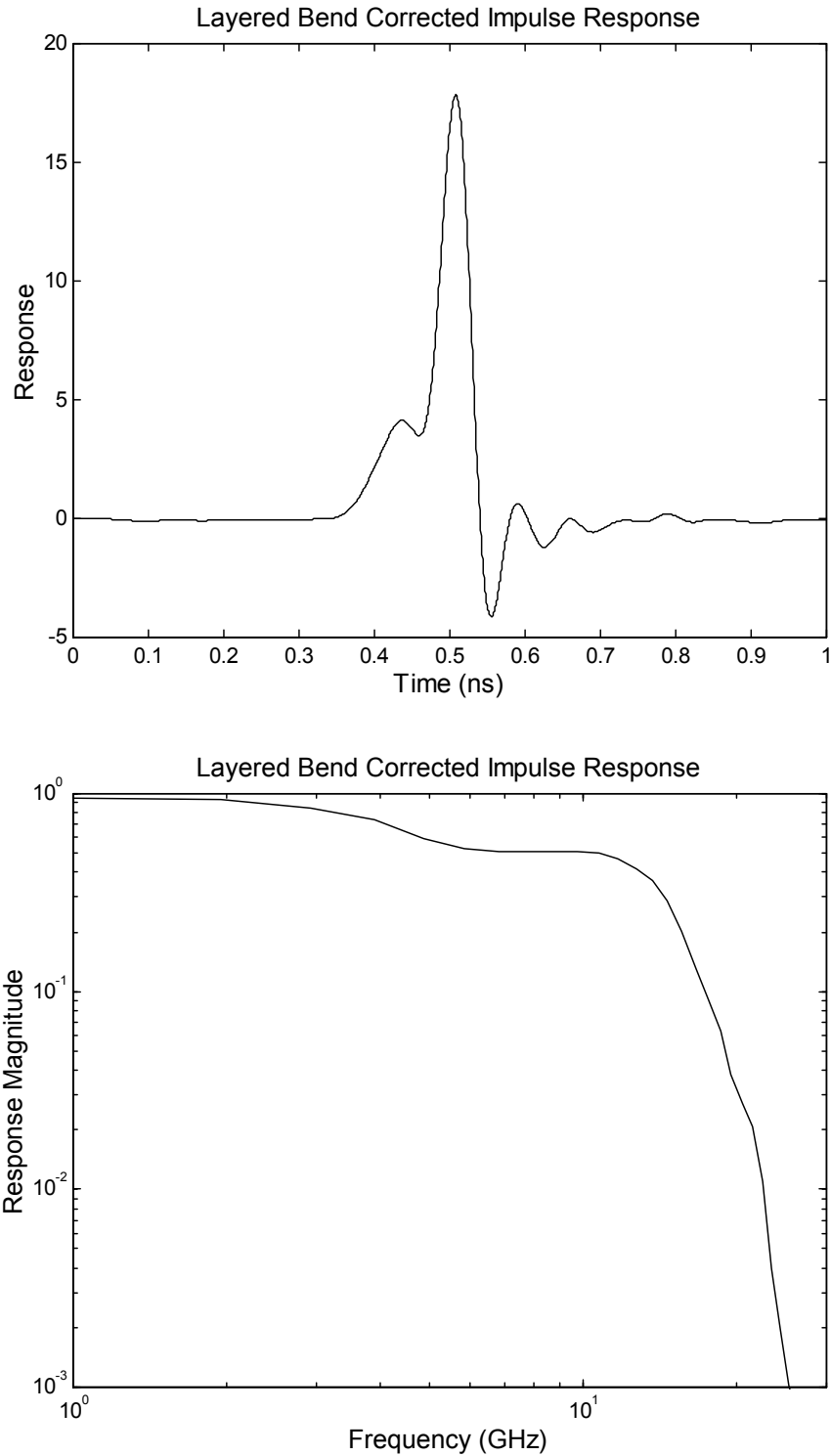
Figure 21. Corrected impulse response for the six-layer laminated bend. The FWHM of the time-domain peak is 44 ps, only 4 ps wider than the corrected response for the comparable straight section of transmission line filled with a uniform dielectric. A 5th order modified Butterworth filter with a 15 GHz cutoff was used in deconvolving the system response from the raw data.

6. Concluding Remarks

This paper has described the design of a test fixture for use in comparing impulse propagation through straight and curved sections of electrically large, square coaxial transmission line. Coaxial geometry was chosen to eliminate fringe fields that limited the performance of a previous strip line device. We designed a layered gradient-index dielectric lens to compensate a transmission line bend, and subsequently analyzed that design by application of a non-linear global optimization algorithm. To investigate a potentially inexpensive compensation approach, based on bends partially filled with uniform dielectric material, we also designed wedge-shaped fillers for the bend hardware.

In the square coaxial transmission line described above, we demonstrated preservation of a fast impulse during propagation through a relatively tight 90° bend, compensated by a six-layer approximation of a CID lens. By applying the global optimization algorithm, we established that the heuristically determined lens design was essentially optimal. In terms of the raw impulse response, the compensated bend increased the pulse width by only 15 ps, to 70 ps, from the 55 ps observed for an equivalent length of straight transmission line. In contrast, without compensation, the transmission line bend distorted the impulse into a bipolar signal spread over a 500 ps time interval.

In contrast to the successful layered bend design, compensation based on partially filling the bend with a shaped uniform dielectric proved futile. Since this approach depended on the orientation of dielectric–air interfaces relative to electric field lines, it might prove useful in a strip line geometry, if the contribution of fringe fields could be neglected.

Appendix A. Optimization of a Layered Approximation of a Graded Index Ultra-Wideband Microwave Transmission Line Bend

We have developed an approach for optimizing the design of layered approximations of CID transmission line bends, based on a commercial non-linear global optimization package for *Mathematica®*. In terms of a continuously varying index of refraction, a true CID bend is described by

$$n = \Psi_{max} / \Psi \qquad (A1)$$

where Ψ is the radius of curvature and Ψ_{max} is the radius corresponding to $n = 1$. The layered approximation replaces this continuous index profile with a histogram of constant-index layers. In searching for the optimum histogram, there may be a range of refractive indices from which to choose, or there may be a set of discrete (stock) values available. In either case, there will be some lack of precision in our knowledge of the individual indices. Reasonable choices for layer radial extents may be impacted by this lack of precision. The selection of layer extents may also be constrained mechanically, by manufacturing limitations. To search objectively for an optimum layer structure, we need a measure of how well the histogram matches (A1).

Since the rise time of a transmitted pulse is directly impacted by any variations in transit time around the bend, it is convenient to use transit time "straggling" or "jitter" as a measure of bend performance. The transit time, as a continuous function of the radius of curvature, through the ith layer of a bend is

$$(\tau)_i = n_i \, \Psi \, \Delta\phi / c \qquad (A2)$$

where n_i is the uniform index of refraction within the layer, c is the speed of light in vacuum, and $\Delta\phi$ is the bend angle in radians. For a CID bend, the transit time is a constant given by

$$\tau_{ref} = \Psi_{max} \, \Delta\phi / c \qquad (A3)$$

The transit time "jitter" can be defined by the difference between (A2) and (A3) as

$$(\Delta\tau)_i = (n_i \Psi - \Psi_{max}) \Delta\phi / c \qquad (A4)$$

For an optimal design, we seek to minimize the variance of the transit time about τ_{ref}, when averaged over all layers in the bend. Thus, it is convenient to choose the root-mean-square (*rms*)

of the transit time jitter,

$$(\Delta\tau)_{rms} = \left\{ \frac{1}{N_l} \sum_{i=1}^{N_l} \frac{\int_{\Psi_{i-1}}^{\Psi_i} (\Delta\tau)_i^2 \, \mathrm{d}\Psi}{\Psi_i - \Psi_{i-1}} \right\}^{1/2} \tag{A5}$$

as the function to be minimized. Using (A4) in the integrand, we finally obtain the *rms* transit time jitter for an N_l-layer bend as

$$(\Delta\tau)_{rms} = \left(\frac{\Delta\phi}{c}\right) \sqrt{\Psi_{max}^2 - \sum_{i=1}^{N_l} \left(\frac{n_i \, \Psi_{max}}{N_l}(\Psi_i + \Psi_{i+1}) - \frac{n_i^2}{3N_l}\left((\Psi_i + \Psi_{i+1})^2 - \Psi_i \, \Psi_{i+1}\right)\right)} \tag{A6}$$

There are constraints on the radii of curvature and indices of refraction, $\{\Psi_i, n_i\}$. The radii must be greater than zero and less than infinity. Also, Ψ_{max} must generally be larger than the width, D, of the transmission line. Thus, we require $0 < \Psi_{i-1} < \Psi_i < \Psi_{max} < \infty$ and $D < \Psi_{max}$. We also require $1 < n_i < n_{i-1} < \infty$. The index will be further restricted by availability of materials. Also, as a practical matter, adjacent layers should probably differ in index by more than the index uncertainty. Through (A1), this difference in indices implies a lower bound on layer width. Manufacturing limitations may suggest yet another lower bound. In combination with D, the minimum layer width suggests a maximum for N_l, although economic constraints may dictate a smaller layer count.

We used the global optimization package for *Mathematica*® to identify sets, $\{\Psi_i, n_i\}$, which minimize (A6). Constraining the optimization only by the physical dimensions of the bend and the chosen dielectric materials, we established that our layered dielectric design is nearly an optimum. The associated *rms* transit time jitter is only 27 ps.

Given only the bend geometry, a list of available dielectric materials (discrete refractive indices), and a maximum number of layers to use, our implementation of the global optimization package can locate optimal layered dielectric parameter sets, $\{\Psi_i, n_i\}$. Even Ψ_{max} can be included among the variables to be determined. If necessary, the optimization process can be tailored to incorporate additional constraints or goals, such as minimum layer thickness and layer-thickness-weighted average refractive index (or dielectric constant).

References

1. W. S. Bigelow and E. G. Farr, "Minimizing Dispersion in a TEM Waveguide Bend by a Layered Approximation of a Graded Dielectric Material," Sensor and Simulation Note 416, 5 January 1998.

2. W. S. Bigelow, and E. G. Farr, "Minimizing Dispersion in a TEM Waveguide Bend by a Layered Approximation of a Graded Dielectric Lens," p. 213-219 in *Ultra-Wideband, Short-Pulse Electromagnetics 4*, E. Heyman, B. Mandelbaum, and J. Shiloh (eds.), Kluwer Academic / Plenum Publishers, New York, 1999.

3. C. E. Baum, "Two-Dimensional Inhomogeneous Dielectric Lenses for E-Plane Bends of TEM Waves Guided Between Perfectly Conducting Sheets," Sensor and Simulation Note 388, 14 October 1995.

4. C. E. Baum, "Dielectric Body-of-Revolution Lenses with Azimuthal Propagation," Sensor and Simulation Note 393, 9 March 1996.

5. C. E. Baum, "Dielectric Jackets as Lenses and Application to Generalized Coaxes and Bends in Coaxial Cables," Sensor and Simulation Note 394, 23 March 1996.

6. C. E. Baum, "Azimuthal TEM Waveguides in Dielectric Media," Sensor and Simulation Note 397, 31 March 1996.

7. C. E. Baum, "Discrete and Continuous E-Plane Bends in Parallel-Plate Waveguide," Sensor and Simulation Note 399, 1 May 1996.

8. C. E. Baum, "Use of Generalized Inhomogeneous TEM Plane Waves in Differential Geometric Lens Synthesis," Sensor and Simulation Note 405, 5 December 1996.

9. C. E. Baum, "Admittance of Bent TEM Waveguides in a CID Medium," Sensor and Simulation Note 436, 2 May 1999.

10. W. S. Bigelow and E. G. Farr, "Impedance of an Azimuthal TEM Waveguide Bend in a Graded Dielectric Medium," Sensor and Simulation Note 428, 21 November 1998.

11. *Reference Data for Engineers: Radio, Electronics, Computer, and Communications*, 8th Ed., p. 20-22, SAMS, Prentice Hall Computer Publishing, Carmel, Indiana 46032, 1993.

Acknowledgment